CityZen

megaCITY - Zoom for the Environment

Collaborative Project

7th Framework Programme for Research and Technological Development

Cooperation, Theme 6:

Environment (including Climate Change)

Grant Agreement No.: 212095

Deliverable 2.4.1b, type R

Impact of emission changes on climate

Due date of deliverable: project month 30

Actual submission date: project month 36

Start date of project: 1 September 2008 Duration: 36 months

Name of lead beneficiary for this deliverable: FZJ

Scientist(s) responsible for this deliverable: Cornelia Richter and Martin Schultz

Project co-funded by the European Commission within the Seventh Framework Programme (2007-2013)		
Dissemination Level		
PU	Public	X
PP	Restricted to other programme participants (including the Commission Services)	
RE	Restricted to a group specified by the consortium (including the Commission Services)	
CO	Confidential, only for members of the consortium (including the Commission Services)	

1 Introduction

There is no doubt any longer that anthropogenic emissions from fossil fuel burning, deforestation and other processes are leading to global warming (IPCC, 2007). Less certainty exists about the consequences of climate change, but there are a number of "fingerprints" which are likely associated with climate change and begin to be observable even now:

1. Changes in precipitation patterns may lead to extended droughts in several regions of the world (e.g. Eastern Africa, central North America). There are real dangers that water supply in these areas will not sustain human settlement in the future. In other regions, precipitation is likely to increase, mainly in the form of massive precipitation events which cause flooding and damages to crops, buildings and infrastructure.
2. Warmer and drier summers, as predicted for central Europe for example, are likely to cause more frequent severe heat waves with elevated death toll as in the example of the summer 2003 event.
3. The warming of sea water and the melting of land ice causes the sea level to rise. Coastal areas and small islands will be prone to flooding and they will be more vulnerable to storm tides. This affects large numbers of people, because coastal areas have become densely populated during the 20th century.
4. The melting of glaciers will reduce freshwater supply in some areas thereby threatening or aggravating the sustainability of drinking water and agricultural water use. While water availability throughout the year may sometimes remain almost unchanged, alterations in the seasonal cycle might bear similar consequences when prolonged drought episodes become more frequent.

Currently, about 7% of the world's population lives in agglomerations with more than 10 million inhabitants (source: *Thomas Brinkhoff: The Principal Agglomerations of the World,* http://www.citypopulation.de, as of April 2011). Several of these megacities are located in regions which are particularly prone to feel the consequences of climate change and the population of megacities is extremely dependent on the supply of freshwater. The urban heat island effect exacerbates the consequences of summer heat waves (see also: CityZen Milestone report M-2-4-1 and references therein, or (Deely et al., 2010). Climate change might also have an impact on the development of megacities themselves. Megacity growth rates will depend on the number of people who arrive from rural areas, for example because they have to abandon their land as a consequence of droughts. Conversely, city dwellers are also responsible for a significant share of the global greenhouse gas emissions. It is difficult to estimate the exact share of megacity emissions due to several conflicting factors:

1. Standard-of-living is often higher in megacities implying that more energy is consumed per inhabitant and more CO_2 emissions are generated.
2. Megacities import goods (in particular food) from other regions so that emissions generated during the production of these goods should be counted as megacity emissions as well and simple emission estimates from rural areas will overestimate the contributions of the rural population.
3. Technology is often more advanced in cities, which means that (fossil) fuel is used more efficiently and fewer emissions are generated for the same amount of "work" done. However, current emission inventories generally assume a uniform distribution of emission factors throughout a country or district.

4. Transportation pathways are longer in rural areas so that delivery of goods from A to B may generate more emissions outside of city regions. On the other hand the globalization of the economy has led to vastly increased transportation pathways for many goods and (mega)city inhabitants might consume more and different goods than the rural population so that they are responsible for a larger share of the (global) emissions from transportation.

Assessing the climate impacts on megacities and the effects of megacities on climate is therefore a very complex task which will require a lot more research than what could be accomplished in the CityZen project. Governments have realized that intelligent urban planning and adaption to climate change impacts are urgently needed in order to minimize the vulnerability of megacities and their contribution to climate change (see for example the German Federal Ministry of Education and Research programme "Research for Sustainable Development of the Megacities of Tomorrow – Energy and Climate Efficient Structures in Urban Growth Centres", http://www.emerging-megacities.org).

In this report we present results from two sensitivity studies performed with the ECHAM5-MOZ and ECHAM5-HAM chemistry climate models in order to assess the impacts of climate change on air quality (with a focus on Europe) and the impact of megacity emissions on the global distribution of aerosols and the resulting radiative forcing. Contrary to the expectation at the writing of the CityZen proposal, it was not possible to perform these simulations with the new version of the model (ECHAM6-HAMMOZ) which would have included more interactions between gas-phase chemistry and aerosols and additional feedbacks from chemistry on radiation. The following sections provide a brief overview on tropospheric chemistry and aerosol processes which may help in the interpretation of the model results. We then chose to highlight the problem of statistical significance which is crucial for the analysis of trends and the assessment of likelihood of a specific phenomenon. Unfortunately, chemistry climate models are still very expensive to run so that there are practically no studies available which explore the uncertainties in a statistically robust manner. Next we describe and interpret the results from our simulations and finally we offer some conclusions.

1.1 Trace gases and atmospheric chemistry

Tropospheric oxidants and other air pollutants have much shorter lifetimes than the prominent greenhouse gas CO_2. Therefore their concentrations vary regionally and the impacts of these substances on weather patterns and vice versa will carry regional signatures and may often not be visible on the global scale. Nonlinearities in atmospheric chemistry complicate the assessment of potential changes, in particular if projected changes in regional emissions are large. A prominent example in this context is the photochemical ozone production. A simplified scheme of tropospheric ozone formation is shown in Figure 1 (Richter, 2008).

Elevated ozone concentrations in the troposphere, part of the so called summer smog, are build during the degradation of volatile organic compounds (VOCs). The presence of sunlight and nitrogen oxides $NO_x = NO + NO_2$ as a catalyst are another prerequisite. The VOCs are oxidized by hydroxyl radicals OH and from organic peroxy radicals RO_2. These organic peroxy as well as later on the hydroperoxy radicals HO_2 react with nitrogen oxide NO. The peroxy radicals release an oxygen atom to become organic oxyl RO and hydroxyl radicals OH, respectively. The oxygen atom in turn is picked up by NO with nitrogen dioxide NO_2 as the product. The organic oxy radical decomposes, isomerizes, or reacts with oxygen. This results in a carbonyl product (organic compound with a C=O group being part of it) and a hydroperoxy radical. The nitrogen dioxide, which is built as a

side product of the VOC degradation, is decomposed by a photon hν. NO is rebuilt and the separated oxygen atom O combines with an oxygen molecule O_2 to form ozone O_3.

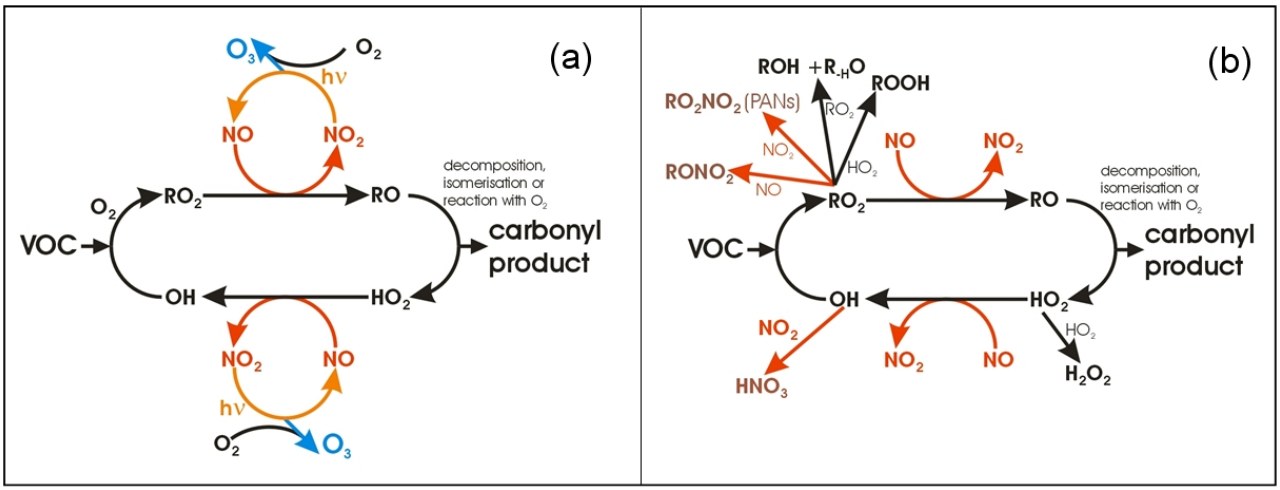

Figure 1 Photochemical ozone (O_3) production in the troposphere. (a) A chain reaction, which involves mainly anthropogenic nitrogen oxides (NO_x = NO + NO_2) and volatile organic compounds (VOCs), leads to the buildup of ozone O_3. Sunlight, symbolized as hν, is needed, to keep the cycle running. The VOCs are oxidized yielding carbonyl products. (b) Various chain termination reactions remove NO_x and/or the radicals (RO_2, HO_2, or OH) from the cycle. New radicals have to be build. Normally this happens by the photolysis of ozone, HONO, or aldehydes (not shown in the figure).

This chain reaction with the recycling of OH and NO is quite complex already. What makes things even more complicated are the chain termination reactions, which remove NO_x and/or radicals from the chain. For example adding NO_x to the system does not necessarily cause the cycle to run faster and accelerate the ozone build-up. The opposite, namely a deceleration of the ozone creation can happen, too, as among others the reaction of NO_2 with OH becomes more important then. Less OH is available for the initial step of the VOC degradation. The whole cycle runs slower. In contrast to naïve expectation, the increase of a precursor species lowers the ozone production rate in this so called VOC limited regime (low VOC to NO_x ratio). In this regime a lowering of the mainly anthropogenic NO_x emissions elevates the ozone production. In the NO_x limited regime (high VOC to NO_x ratio) however, a lowering of NO_x emissions reduces the ozone production. In the CityZen brochure available at https://wiki.met.no/cityzen/start the change of the regime of the London air pollution is illustrated. CityZen results on the influence of model resolution on this issue (low resolutions wipe out concentration peaks of trace gases due to the averaging over huge areas) are published in a recent CityZen publication (Hodnebrog et al., 2011).

1.2 Aerosols

Aerosols have natural and anthropogenic sources, can be emitted directly as particles (primary aerosols) or can form in the atmosphere from gaseous precursor species (secondary aerosols). Over sea and in costal areas, seasalt aerosols from sea spray are important. Mineral aerosols are particles picked up by wind from dry surfaces, especially surfaces without a shielding plant cover. Although these particles are rather big (diameters of 10µm and above), thus heavy compared to their surface and liable to gravity, they can reach quite far depending on the wind field. Sahara dust events in central Europe are one example for that. Marine and mineral aerosols belong to the coarse mode aerosols. In the CityZen focus of interest region Istanbul, the mass of seasalt and crustal particles

made up nearly 20% of the observed mass in the period between November 2007 and June 2009 (Koçak et al., 2010). Volcanic eruptions are another important source of aerosols. Biogenic aerosols are particles produced by living organisms, e.g. pollens, fungi spores, bacteria, and viruses. Naturally occurring or humanly induced biomass burning is another temporally highly variable and massive source of (ash) aerosols. Human activities evoke emissions of primary aerosols, too. Fossil fuel combustion in various facilities like vehicles, power plants or for industrial purposes is the source for fine anthropogenic aerosols. Construction sites or abrasion at tires and brakes of road vehicles are sources for coarse aerosols. Gaseous precursor species, which may form secondary aerosols by nucleation or condense on pre existing particles, are emitted by the biosphere as well as by anthropogenic processes. An estimate of the global source strength as well as the global mean optical thickness at 550nm, which is a measure for the global load as well as the influence on the radiative budget of planet earth, is given in Table 1.

	Main sources for aerosol *Estimates of Andreae (1994)*	Approx. global emission flux [Tg / year]	Global mean optical thickness at 550 nm
Natural	***Primary aerosols***		
	Desert and semi-arid areas (mineral dust)	1500	0.023
	Marine sea spray	1300	0.003
	Volcanic dust	33	0.001
	Biogenic (pollens, debris)	50	0.002
	Secondary aerosols		
	Sulphates from biogenic gases	90	0.017
	Sulphates from volcanic SO_2	12	0.002
	Nitrates from nitrogen oxides	55	0.017
	Organics from volatile organic compounds (VOC)	22	0.001
	TOTAL	***~3060***	***0.066***
Anthropogenic	***Primary aerosols***		
	Industrial dust	100	0.004
	Soot	10	0.006
	Secondary aerosols		
	Organics from biogenic (VOC)	10	0.027
	Sulphates produced by SO_2	190	0.027
	Produced from biomass combustion gases	90	0.002
	Nitrates from nitrogen oxides	50	0.003
	TOTAL	***~390***	***0.069***

Table 1: Aerosol sources and global mean optical depths of aerosols according to the literature.

Aerosols from cloud condensation nuclei and as such influence the Earth's climate. One differentiates between direct aerosol effects on radiation (the scattering and absorption of solar and longwave radiation on and by aerosol particles themselves) and indirect effects which are related to changes in cloud albedo (higher aerosol densities will lead to smaller cloud droplets which increase cloud brightness), cloud lifetime (smaller droplets are less likely to precipitate so that aerosol-rich clouds may live longer) and other feedbacks such as changes in buoyancy which affect the altitude to which clouds may rise.

1.3 A note on statistics

In order to assess climate change and its impacts it is not sufficient to only consider average quantities such as the global mean temperature. While these values can at times be meaningful, they often hide what is really happening and may imply consequences that are less harmful than they really are. One example from recent work under the task force of hemispheric transport of air pollution (Fiore et al., 2009) are changes in surface ozone concentrations that are induced by moderate regional emission changes of ozone precursors. While annual average changes are generally very small, they hide the much larger compensating differences in summertime and wintertime ozone concentrations.

Figure 2 shows the probability density function of the Gauss distribution for three different mean values μ and standard deviations σ. Many atmospheric state variables exhibit frequency distributions that are very close to a gaussian distribution. The area under the curve between X_0 and X_1 represents the probability of the random variable to assume a value between these limits (the total area is 1). An area of about 0.95 lies between -2σ to +2σ around the mean μ. This means that the random variable will fall into this range with a probability of 95% during a concrete experiment or observation. To phrase this differently: out of 100 simulated climate years, 5 years will show "atypical" results. Much smaller sample sizes (e.g. 10 years) are not sufficient to obtain a robust description of the statistical distribution and to assess if an observed change was indeed significant.

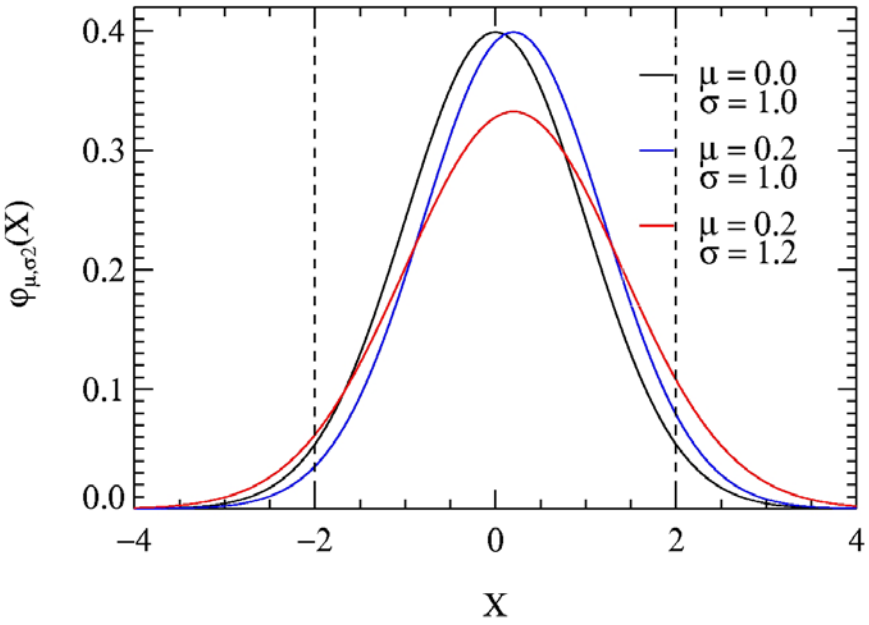

Figure 2 Probability density function φ of the Gauss distribution for three different pairs of mean values μ and standard deviation σ.

The accurate determination of the parameters of the distribution function is especially important to assess climate extremes. For example: The black curve in Figure 2 shows the standardized normal distribution with a mean value μ_0 of zero and a standard deviation σ_0 of one. The 2σ interval for this standardized normal distribution is marked with dashed lines. The probability for extreme events outside this interval is about 5% (2.5% for extreme values below $\mu_0-2\sigma_0$ and 2.5% for values above $\mu_0+2\sigma_0$). Increasing the mean value of the distribution shifts the distribution to higher values (blue curve). Extremely low values below $\mu_0-2\sigma_0$ are less probable for this case (the blue curve lies below the black), the probability for extremely high values above $\mu_0+2\sigma_0$ rises (blue curve is above the black). If not only the mean value rises but also the variability σ^2 (red curve), the probability for extreme events may rise not only at one end of the distribution but on both (red curve is above the black outside the $2\sigma_0$ interval). Referring to the example of temperature deviations this means that

rising climate variability elevates the probability of extremely cold temperatures although the global mean temperature rises.

A high variability of observed climate or air quality variables makes it difficult to assess small trends in the timeseries of these variables. Long timeseries are needed to find "real" trends, which are statistically significant and not only a misinterpretation of inter-annual variability. This is demonstrated in Figure 3.

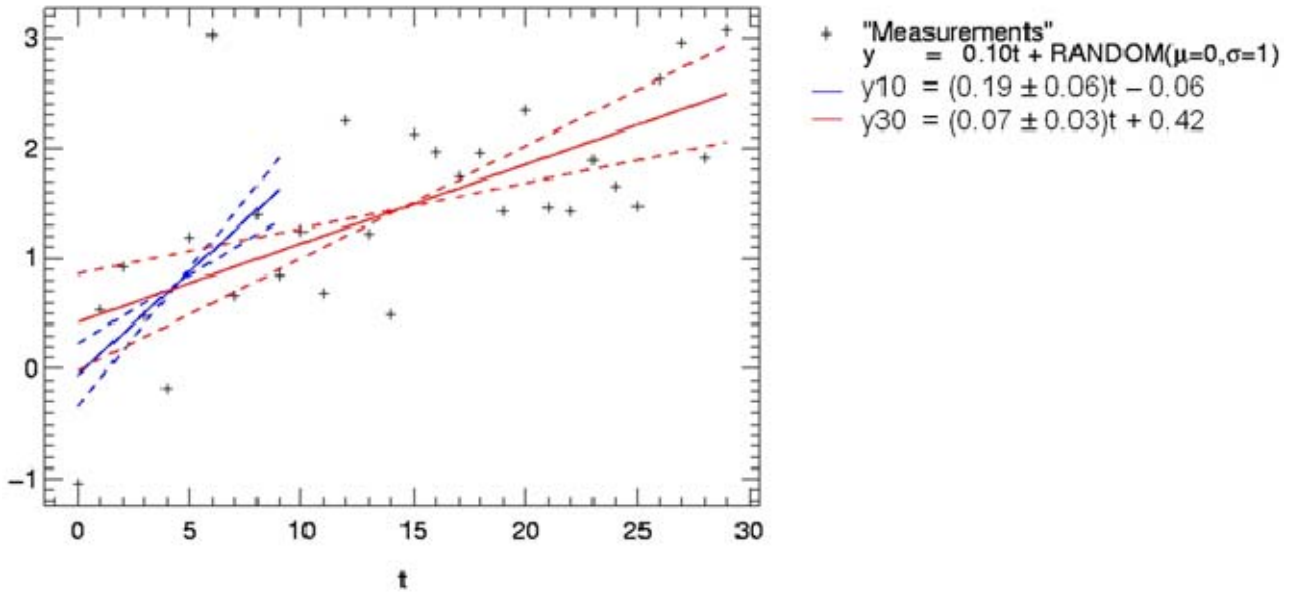

Figure 3 Regression lines in a highly variable fictitious timeseries. The timeseries has an underlying small trend (0.1 per timestep). If only a short interval (10 timesteps) is looked at, a quite different "trend" will be found compared to the one determined with the longer timeseries (30 timesteps).

The fictitious timeseries in Figure 3 was built by adding randomly normal distributed deviations (μ=0, σ=1) to a small trend of 0.1 per time step. Two regression lines are deduced by a linear least square fit. The first one (blue) uses the first 10 timesteps only. A much larger trend is found in this case. Actually the 95% confidence interval[1] of the fitting line's slope does not cover the underlying prescribed (real) gradient of the fictitious "measurements" in this example case. If 30 timesteps are taken into account for the regression analysis, the slope of the fitting line is much closer to the real trend. The 95% confidence interval of the fitting line slope just covers this real trend. In reality, the underlying real trend is unknown, but has to be derived from the timeseries. The higher the residual variance around the fitting line, the longer timeseries are needed. If the reason for the residual variance is known and the effect of underlying process can be foreseen, thus it is not a random deviation from the trend line, this part of the variation should be removed. For example, if a timeseries shows a strong seasonality, it is appropriate to look at the trend of each season separately or to deseasonalize the time series prior to the trend analysis. Additional complications arise if – as in the case of tropospheric ozone – there are indications that the trend is in fact non-linear.

[1] From the slope of the regression line b, the residual variance around this line s_b (assumed as being Gauss distributed), and a hypothesis for the slope b_0, the variable t_b can be defined, which is Student-T distributed. The Student-T distribution is a special probability density function, depending on degrees of freedom m. This degree of freedom depends on the sample size (number of measurements). For huge m it is equal to the Gauss distribution. By prescribing a significance level α (for a 95% confidence interval α=5%), a maximum and minimum for t can be calculated from the Student T distribution for m = n-2, with the number of used data points for the regression analysis being denoted as n. From this t_{max} and t_{min} values for b_{0max} and b_{0min} are derived giving the confidence interval for a prescribed α.

2 Impacts of climate variability on air quality in Europe

In order to investigate the impact of weather patterns on air quality in Europe we carried out two long-term simulations covering the period 1989 to 2008 with the ECHAM5-MOZ chemistry climate model. One of the simulations (henceforth called "nudged run") was driven by assimilated meteorological fields (surface pressure, air temperature, vorticity and divergence) from the ERA-Interim reanalysis (ECMWF) while the other simulation was constrained only by a climatology of sea ice and sea surface temperatures ("unnudged run"). In the nudged simulation, the meteorological input fields are read every six hours and the climate state is relaxed towards these fields with e-folding times of 6 to 24 hours. The ECHAM5-MOZ model includes a comprehensive tropospheric trace gas chemistry package but does not account for prognostic aerosols. Meteorology affects trace gas concentrations through feedbacks on chemical reaction rates, photolysis frequencies, emissions, deposition and washout. There is no feedback from the tracer fields to the shortwave or longwave radiative transfer in the climate model.

2.1 ECHAM5-MOZ model description and simulation setup

The 3D global chemistry climate model ECHAM5-MOZ is part of the Max Planck Institute for Meteorology (Hamburg, Germany) earth system model. It consists of the atmospheric general circulation model ECHAM5 and the chemistry transport model MOZART2.

ECHAM5 is the 5th generation general circulation model of the Max Planck institute for Meteorology. It evolved from the ECMWF operational forecast model cycle 36 and a comprehensive physics parameterisation package. Details can be found in (Roeckner et al. 2003). The sensitivity of the ECHAM5 model to different horizontal (T21 - T159 sprectral triangular truncation) and vertical (L19 - L159 levels) resolutions concerning the simulated climate is dealt with in (Roeckner et al. 2006) and concerning tracer transport in (Aghedo et al. 2010). Besides chemistry tracers undergo advection, convective transport, and vertical diffusion as well as wet and dry deposition. For the advection a mass conserving semi Lagrangian transport scheme (Lin and Rood, 1996) on a Gaussian grid is used. Convective transport is parameterized as proposed by (Tiedtke, 1989) with modifications following (Nordeng, 1994). The parameterizations for the wet deposition are adapted from Seinfeld (Seinfeld and Pandis, 1998) and (Stier et al., 2005). The vertical diffusion is extended in ECHAM5-MOZ compared to ECHAM5 to include the net tracer flux of surface emissions minus dry deposition. The dry deposition of ozone, nitrogen oxides and nitric acid vapour is implemented according to the resistance model of (Ganzeveld and Lelieveld, 1995).

The atmospheric chemistry scheme of MOZART2 (**M**odel of **OZ**one **A**nd **R**elated chemical **T**racers, version 2) used in ECHAM5-MOZ consists of 63 species representing ozone, nitrogen oxides and hydrocarbon chemistry in 168 reactions. The solver uses the Euler backward integration method. Details on the scheme can be found in (Horowitz et al. 2003). The photolysis rates are computed by interpolation from a multivariate table. This table originates from calculations with the **T**ropospheric **U**ltraviolet and **V**isible radiation model (TUV, version 3.0) (Madronich and Flocke 1999). The model does not simulate stratospheric chemistry explicitly but relaxes the concentrations of ozone to climatologies from (Logan 1999) for O_3 below 100 mb and the **HAL**ogen **O**ccultation **E**xperiment (HALOE) (Randel et al. 1998) for O_3 above 100 mb. The stratospheric concentrations of $NO_x = NO + NO_2$, HNO_3, N_2O_5, and N_2O are relaxed toward zonally and monthly averaged values from the middle atmosphere model **S**tudy of **T**ransport **A**nd Chemical **R**eactions in the **S**tratosphere (STARS) (Brasseur et al. 1997).

In this study ECHAM5-MOZ was run on a horizontal resolution of T63 (spectral triangular truncation), corresponding to a grid resolution of roughly 150km × 150km. The model has 31 vertical levels (L31) from the surface up to 10hPa. The nudged simulation was driven with analyzed fields of surface pressure, temperature, vorticity, divergence, sea surface temperature, and sea ice cover from ECMWF operational meteorological data in order to reproduce the weather patterns during the period 03 1989 -12 2008. In the unnudged simulation sea surface temperatures and sea ice coverage data were used from (Hurrell et al. 2008).

Anthropogenic trace gas emissions are taken from the ACCMIP inventory (Lamarque et al., 2010). Till the year 2000 the historic reanalysis data are used (the linear interpolation between the given decadal values), from the year 2001 on, the RCP8.5 scenario data are used (Riahi et al., 2007). Biogenic emissions from terrestrial vegetation are computed interactively with the Model of Emissions of Gases and Aerosols from Nature (MEGAN), version 1 (Guenther et al., 2006) using updated isoprene and terpene maps of potential emissions which resemble those of the MEGAN version 2 inventory. The NOx emissions by lightning are computed interactively based on convective updraught velocities following (Grewe et al., 2001). Methane concentrations in the model are constrained with a zonal mean surface climatology in the planetary boundary layer, so that time varying CH4 emissions (e.g. derived from inverse modelling using satellite retrievals (Bergamaschi et al., 2009) only serve to create spatial patterns near the surface.

2.2 Mean values of surface temperature and ozone

In Figure 4 the simulated mean summer (June, July, August) temperatures are shown for the nudged and unnudged run, respectively. With the chosen color scale, the two fields look very similar, indicating that the model is able to capture the mean temperature distribution over Europe rather well in spite of its coarse resolution and the constraint by sea ice and sea surface temperature only. The largest exception occurs in the White Sea where the nudged simulation exhibits 3.5 degree warmer temperatures on average due to less sea ice coverage. The unnudged run is slightly cooler over the western part of the Baltic Sea, parts of France, the Alps and Russia. It is warmer over the Mediterranean and large parts of North Africa (Figure 5).

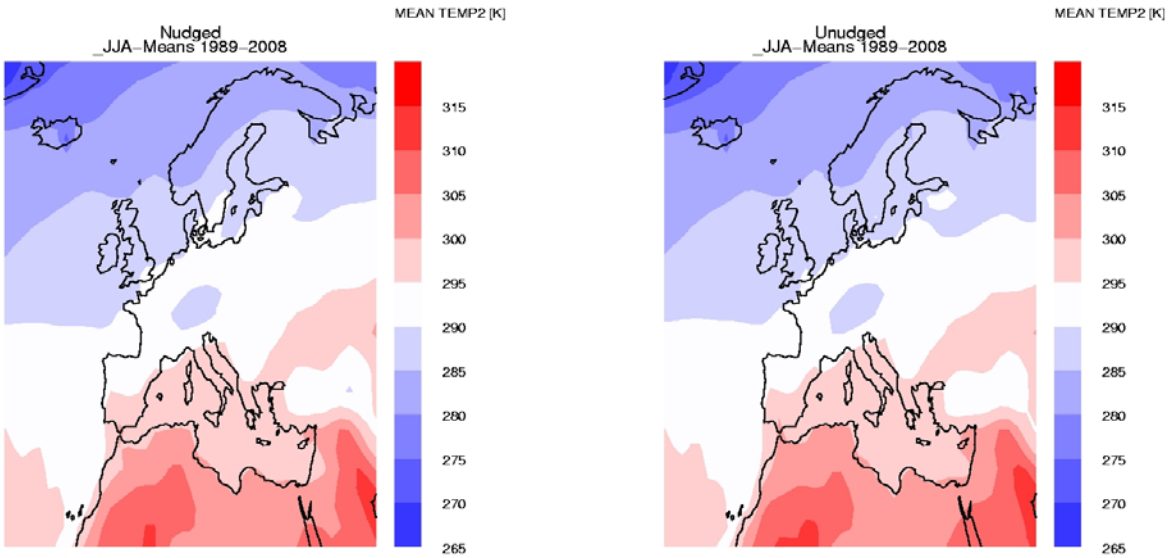

Figure 4 Mean summer 2m-temperature in the nudged (left) and unnudged (right) ECHAM5-HAM simulations.

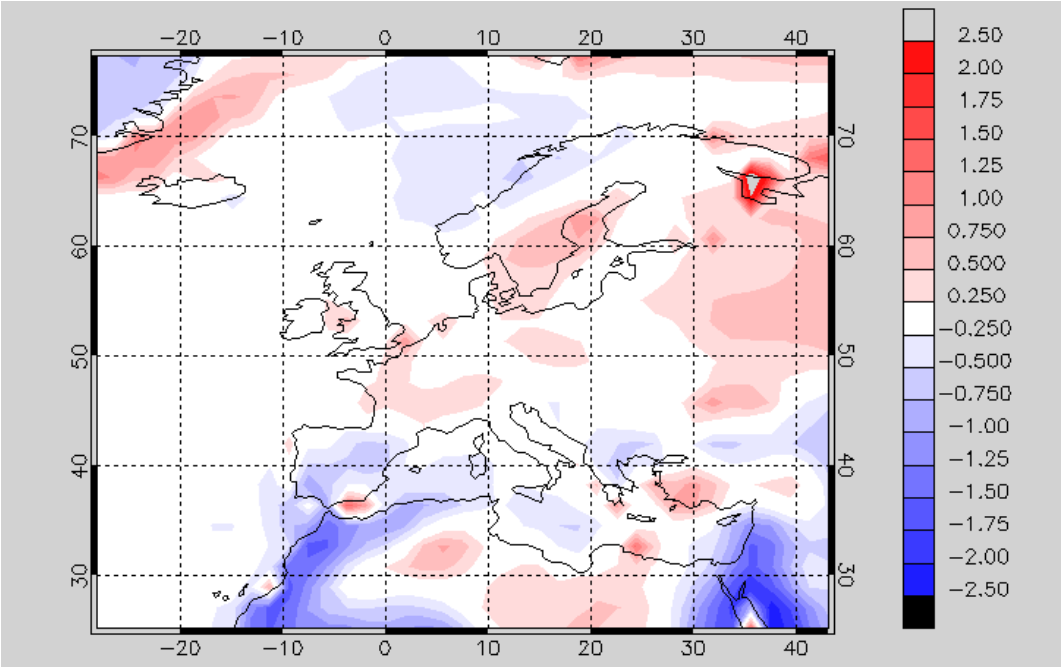

Figure 5 Difference of mean summer 2m-temperatures between the nudged and unnudged simulations [units: K].

Comparing the mean summer ozone concentrations shown in Figure 6 again shows very good agreement between the two simulations. The unnudged simulation tends to yield slightly lower ozone concentrations. Both models agree in placing the highest ozone values in the Mediterranean Sea, where high anthropogenic and biogenic emissions coincide with high sunlight intensity. In contrast to the Eastern Mediterranean results obtained by other groups in the CityZen project, ECHAM5-MOZ does not show significantly larger ozone concentrations in the Eastern Mediterranean region compared to the western region.

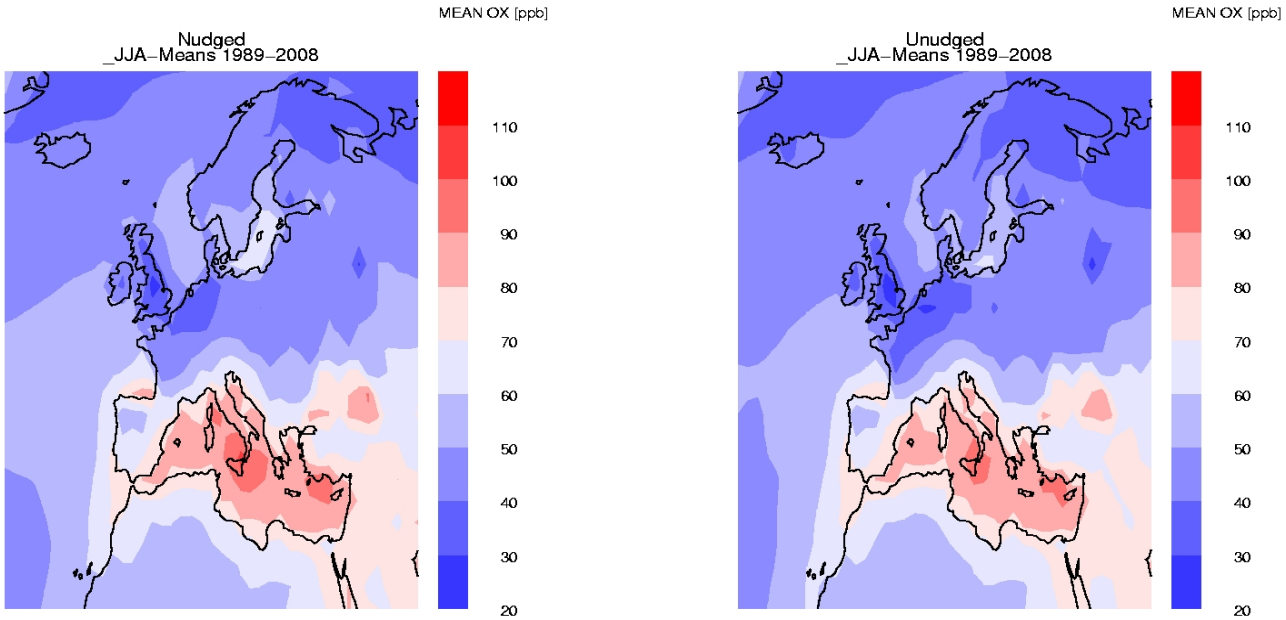

Figure 6 Mean summer surface Ox values. In the unnudged simulation (right) the values tend to be slightly lower.

Figure 7 shows the JJA 20-year mean difference of surface ozone concentrations between the two runs. The nudged simulation yields somewhat larger concentrations in particular in (but not limited to) regions where the average temperature is warmer (see Figure 5).

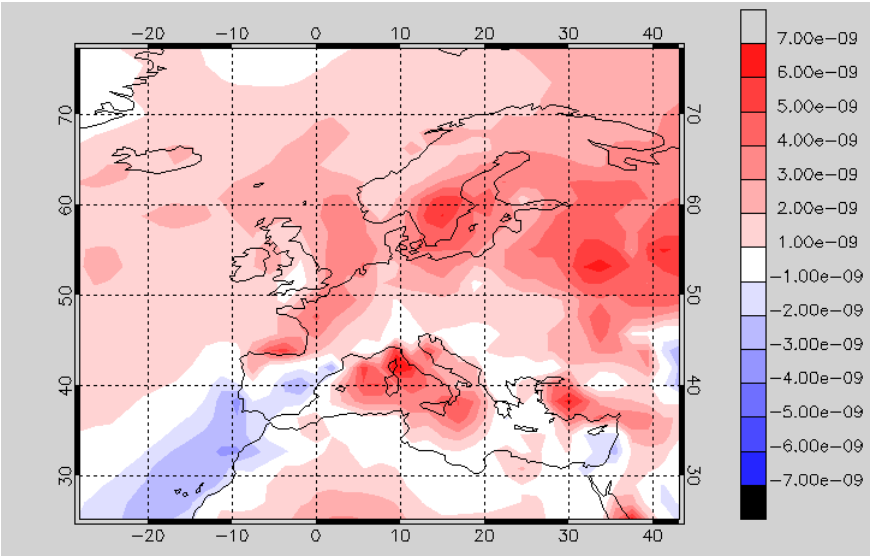

Figure 7 Difference between summer surface Ox values from the nudged and unnudged simulation [units: nmol mol^{-1}].

2.3 Variability

Figure 8 shows the standard deviation of the mean summer temperatures in the nudged and unnudged simulation, respectively. Obviously, the geographical patterns are not equal. Again, the White Sea shows up as an outlier due to differing sea ice coverage. The unnudged simulation exhibits about twice the variability in Spain, southern France and northern Italy than the nudged run and the region of lower variability which stretches across France, Switzerland, Austria, Hungary etc. is shifted to the north.

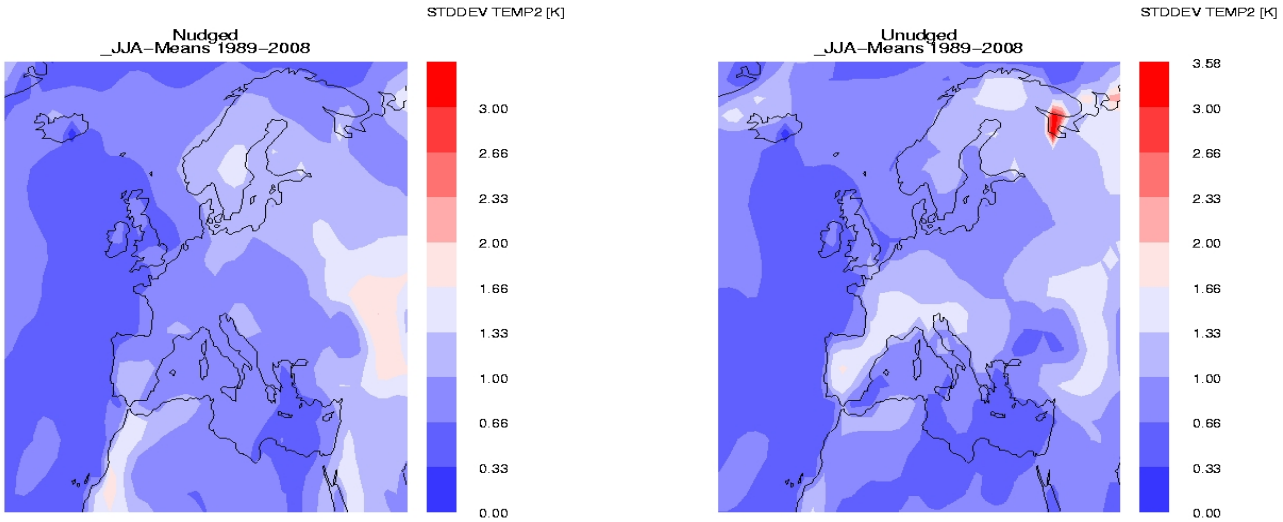

Figure 8 Standard deviation of the 2m-temperature in the summer month (JJA). Left: nudged simulation, right: unnudged run.

Figure 9 displays the difference between the mean 95%-ile and mean median 2m temperatures of the 1990s from the two runs. The 95%-ile and median values were computed from the 3-hourly output for each summer season (JJA) between 1990 and 1999 and then averaged. While the patterns of the "heat episodes" are comparable in the two simulations, the unnudged simulation exhibits somewhat stronger temperature enhancements than the nudged simulation. In theory this should also lead to higher maximum ozone concentrations. However, this is not confirmed (see Figure 7a below).

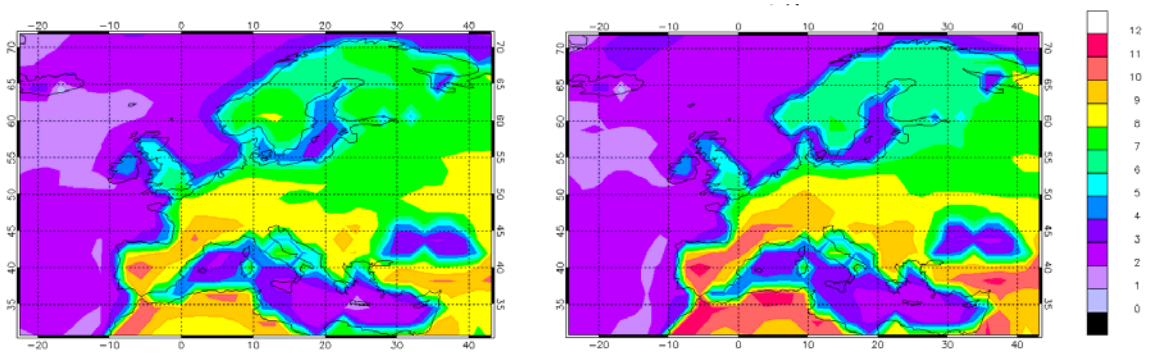

Figure 9 Summertime 2m-temperature enhancements expressed as difference between the mean 95%-ile and mean median values from the nudged (left) and unnudged (right) simulations. [units: K].

Figure 10 shows the mean summer ozone concentration variability. In Eastern Europe, the variability is again underestimated. On the other hand, Figure 11 shows that both simulations yield rather similar "high ozone values", expressed here as 95%-iles computed from the 3-hourly model output. Both the regions and the absolute enhancements of ozone concentrations are very similar in the two runs. The same is true for the low end of the distribution (5%-ile plots in Figure 11).

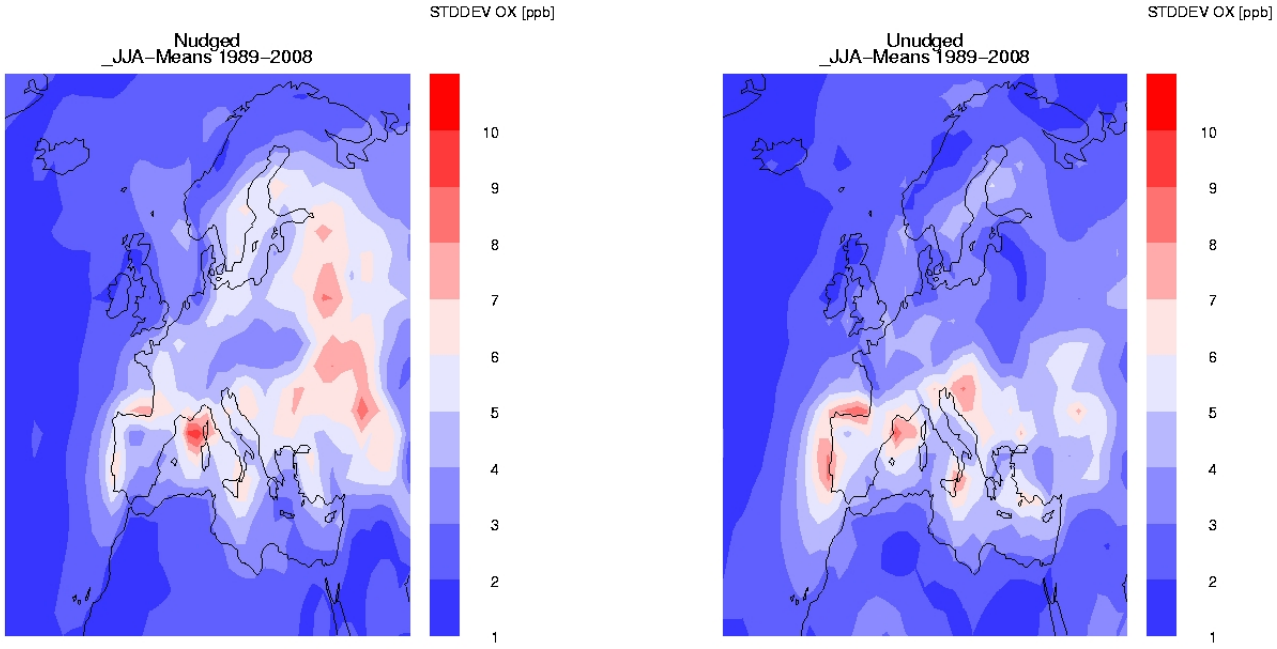

Figure 10 Mean summer ozone concentration variability. In Eastern Europe the variability is highly underestimated.

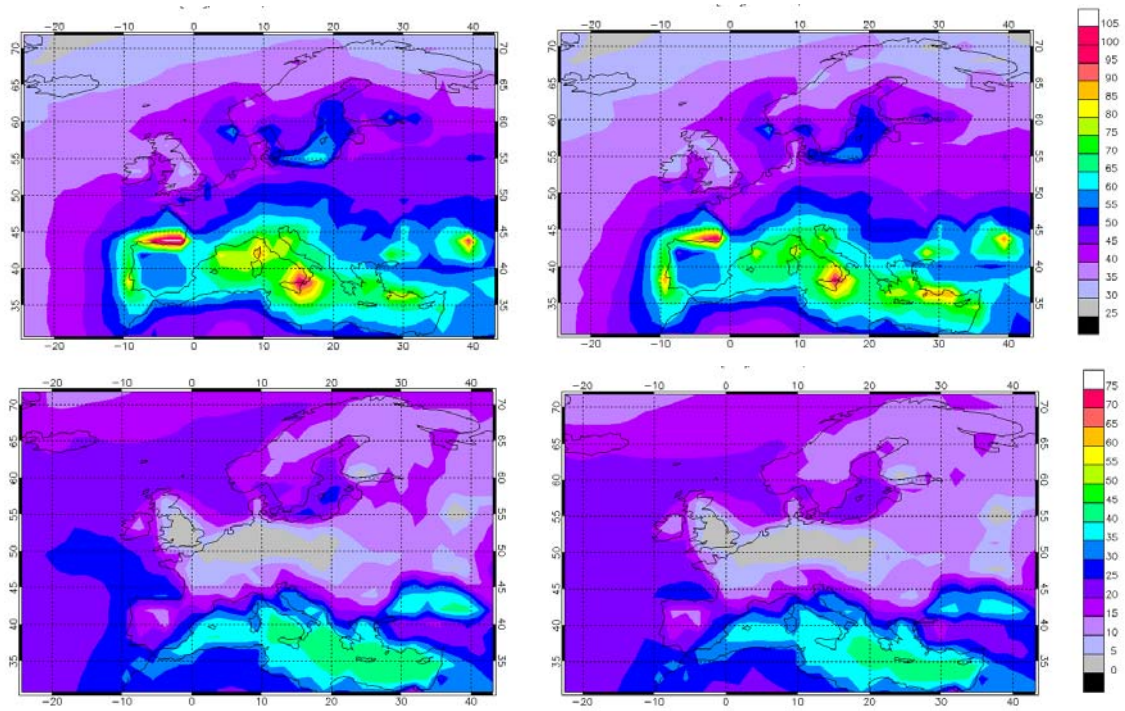

Figure 11 Average summertime 95%-iles (top) and 5%-iles (bottom) of the simulated surface ozone concentration during the 1990s in the nudged (left) and unnudged (right) simulations [units: ppbv].

2.4 Trends

Figure 12 shows the 2m-temperature trends for the summertime (JJA) mean values. Over large parts of central Europe, no significant trend can be detected in either of the simulations. A noticeable difference is the warming of the Iberian Peninsula that is predicted in the unnudged simulation but absent in the nudged simulation. The nudged run exhibits a much larger warming to the east of Europe, while the unnudged simulation shows greater temperature increases in the northern North Atlantic. There are practically no regions where temperature decreased over the past 20 years.

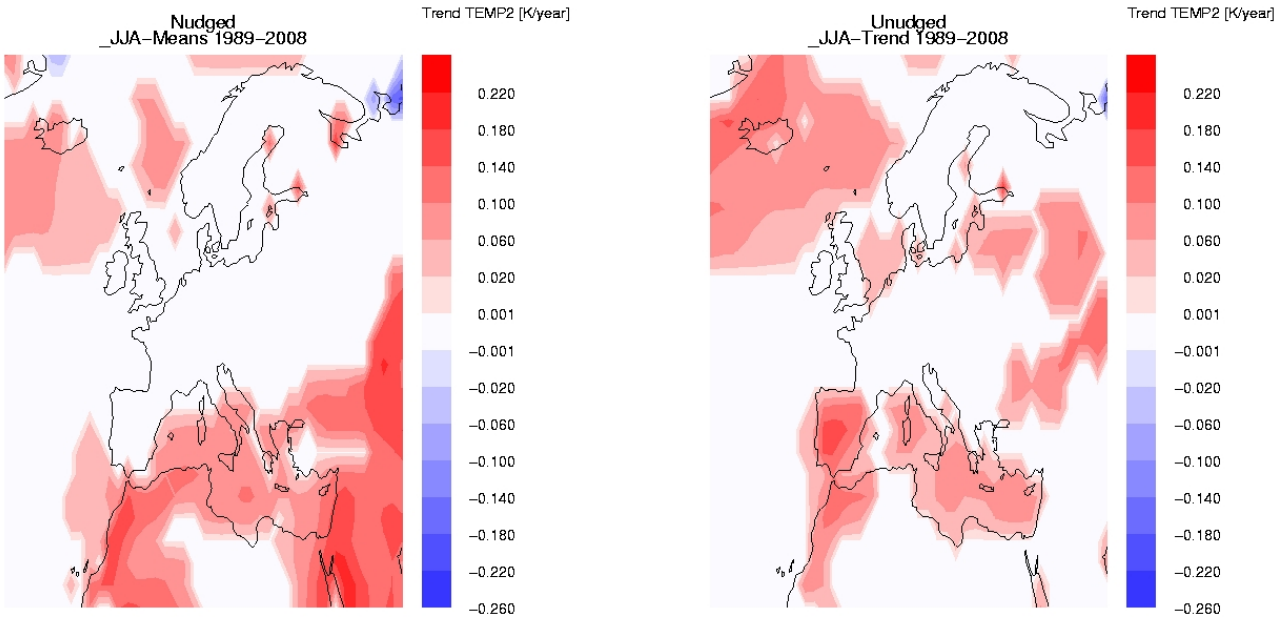

Figure 12 Statistically significant near surface mean summer temperature trends.

Looking at the ozone trends shows a different picture. In the nudged simulation a clear, significant negative trend is visible, whereas hardly any significant trend shows up in the unnudged simulation (Figure 13).

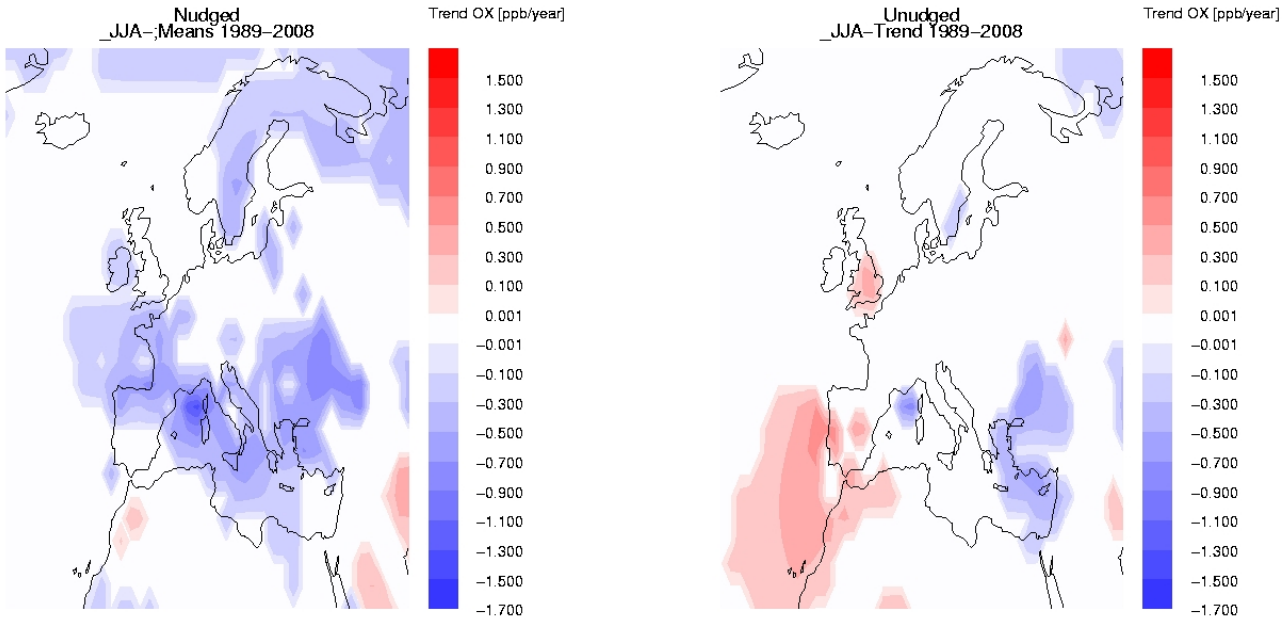

Figure 13 Significant summer ozone concentration trends.

3 ECHAM5-HAM sensitivity runs

Two ten year future (years 2025 – 2035, year 2025 as spin up) scenario simulations were done with the ECHAM5-HAM model. This model deals with aerosols in the atmosphere and their impact on weather elements and climate. A two way coupling is established in this model, thus the weather conditions do not only influence the aerosols' fate, but the aerosols change the weather conditions as well (see chapter 1.2). By switching off the megacities' anthropogenic aerosol emissions in one of the ten year simulations, the influence of megacities on global climate (radiative forcing measures are calculated by the model, too) and on weather elements, especially cloud properties, could be looked at.

3.1 ECHAM5-HAM model description and simulation setup

The ECHAM5-HAM model consists of the same general circulation model ECHAM5 as the above described ECHAM5-MOZ. Instead of the chemistry transport model MOZART, the ECHAM5 is coupled with the Hamburg Aerosol Model HAM. The model is described in (Stier et al., 2005) in detail. Here only a short introduction is given.

For computational efficiency, the aerosol spectrum (see chapter 1.2) is divided into seven modes (four soluble and three insoluble modes). They are classified as given in Table 2. Five different aerosol cpecies are considered, namely sulphate, black carbon, organic matter, dust and seasalt. The smallest fraction of particles in the model only consists of soluble sulfur (SU) particles. This fraction is called nucleation mode with particle radii below 0.005µm. In the Aitken mode with radii between 0.005 and 0.05 µm, sulfur, black carbon (BC) and particulate organic matter (POM) are dealt in the soluble / mixed state and additionally insoluble fractions of BC and POM. In the accumulation mode (0.05 – 0.5 µm), sulfur, black carbon, particulate organic matter, sea salt (SS) and dust (DU) particles are dealt in the soluble/mixed state and dust particles in the insoluble mode. In the coarse mode, radii above 0.5 µm, the same particles as in the coarse mode are simulated.

Modes $\bar{r}$ [µm]	**Soluble / Mixed**	**Insoluble**
Nucleation		
$\bar{r} \leq 0.005$	N_1, M_1^{SU}	
Aitken		
$0.005 < \bar{r} \leq 0.05$	$N_2, M_2^{SU}, M_2^{BC}, M_2^{POM}$	N_5, M_5^{BC}, M_5^{POM}
Accumulation		
$0.05 < \bar{r} \leq 0.5$	$N_3, M_3^{SU}, M_3^{BC}, M_3^{POM}, M_3^{SS}, M_3^{DU}$	N_6, M_6^{DU}
Coarse		
$0.5 < \bar{r}$	$N_4, M_4^{SU}, M_4^{BC}, M_4^{POM}, M_4^{SS}, M_4^{DU}$	N_7, M_7^{DU}

Table 2 Aerosol modes in HAM. N_i denotes the aerosol number of mode i, M_i^j the mass of mode i of compound j. The different compounds are: SU (sulfur), BC (black carbon), POM (particulate organic matter), SS (sea salt), and DU (dust). The mode borders are defined via the radius of the particles r. For some compounds not only soluble of mixed but also insoluble aerosols exist. The table is copied from (Stier et al. 2005)**.**

Beside the direct emissions, particles undergo sedimentation, wet and dry deposition. In the microphysics module, nucleation (building of new particles from gaseous precursors), coagulation (combination of two or more preexisting particles), and condensation of gaseous tracers onto existing aerosols is treated.

The model was run in T63L31 resolution. As mentioned above, the simulations started Jan 2025 for a one year spin up and lasted till the Dec 2035. The ocean boundary conditions sea surface tem-

perature and sea ice coverage were taken from coupled ECHAM5-OM simulations of the A1B scenario for the 4th IPCC report. Natural emissions of dust, (dry) salt, dimethyl sulfide (DMS) are deduced from the calculated wind fields. Continuous and explosive volcanic SO2 emissions and organic matter (SOA) emissions are prescribed by constant input files. For the biomass burning emissions, inventory files for the years 1997-2002 were cyclically used. For details: (Stier et al., 2005). The anthropogenic emissions of organic carbon (OC), black carbon (BC), and SO2 were taken from the ACCMIP RCP 8.5 scenario (Riahi et al., 2007), more precisely the linear interpolations between the given decadal values. In the reference run all emissions were kept as given, in the "MC off" scenario, all anthropogenic "Megacity" emissions were switched off. As any city borders are not known for the future, the predicted population density (by Vadim Chirkov, IIASA) for the year 2030 on a 0.5°× 0.5° grid was used. Every grid cell with a population density above 150 inhabitants per km^2 was assigned to be a "megacity grid cell", see Figure 14. The anthropogenic emissions in these grid cells in the ACCMIP.8.5 files with 0.5°× 0.5° resolution were set to zero and after that, the emission files were interpolated to the T63 model resolution.

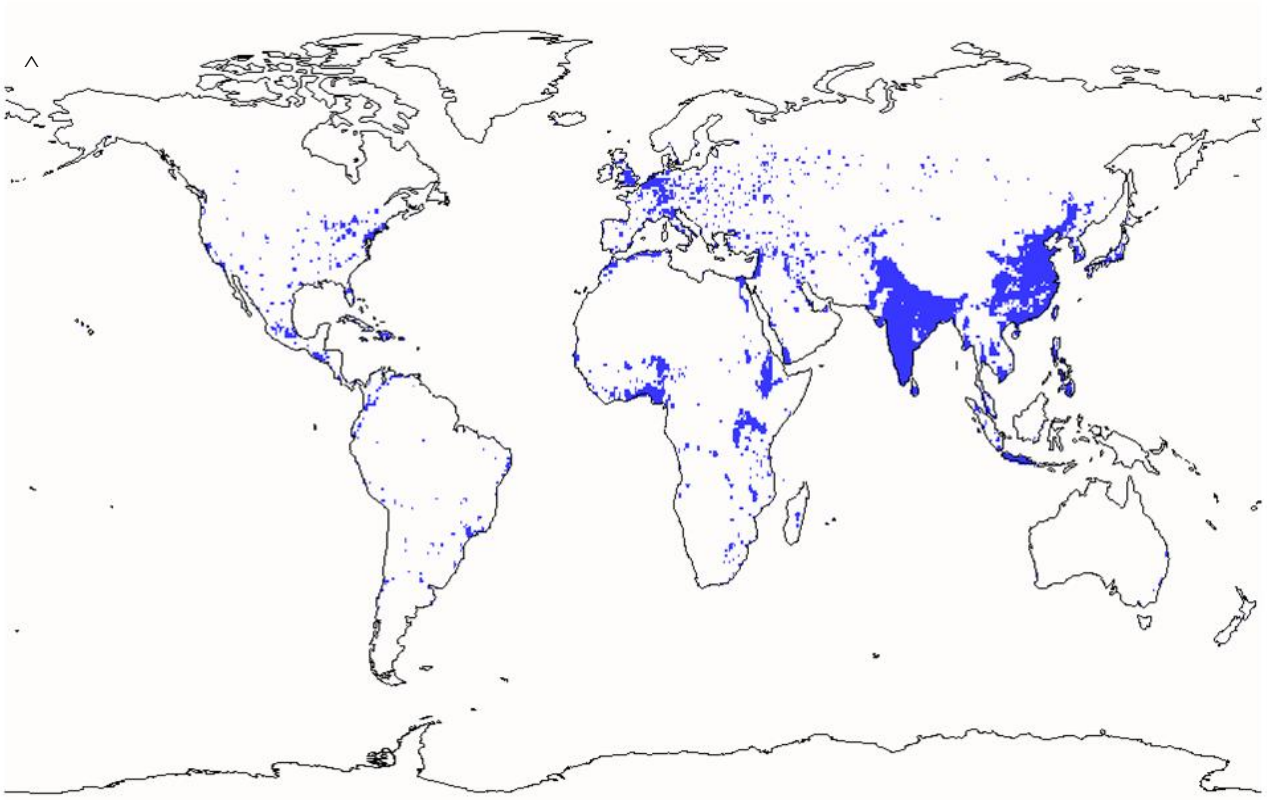

Figure 14 "Megacity" mask for the year 2030 used for switching of anthropogenic megacity emissions in the ACCMIP RCP 8.5 emission files. In the 0.5°× 0.5° grid cells a threshold of 150 inhabitants per km^2 was used.

3.2 Results

As shown above ECHAM5 does a quite good job in predicting mean values but doesn't perform very well concerning variability or trends, if the modeling period is to short and the ensemble to small. As the modeling period is even shorter this time (only ten years instead of 20) and no ensembles but only a single run has been performed for the reference and the "MC off" scenario, respectively, we will only look at decadal mean values in the following.

Figure 15 displays the top of the atmosphere (TOA) and surface (SUR) direct aerosol radiative forcing from the base case simulation. As explained in IPCC, 2007, aerosols with some absorbing component lead to negative TOA forcing over dark surfaces (e.g. oceans), while they can exhibit slightly positive TOA forcing over bright surfaces. The minimum forcing is -20 W m^{-2} over the

tropical Atlantic while the maximum (positive) forcing is +5.3 W m^{-2} over the Sahara. Aerosols always cool the surface (Figure 13 right panel). The minimum SUR forcing is -32.5 W m^{-2}.

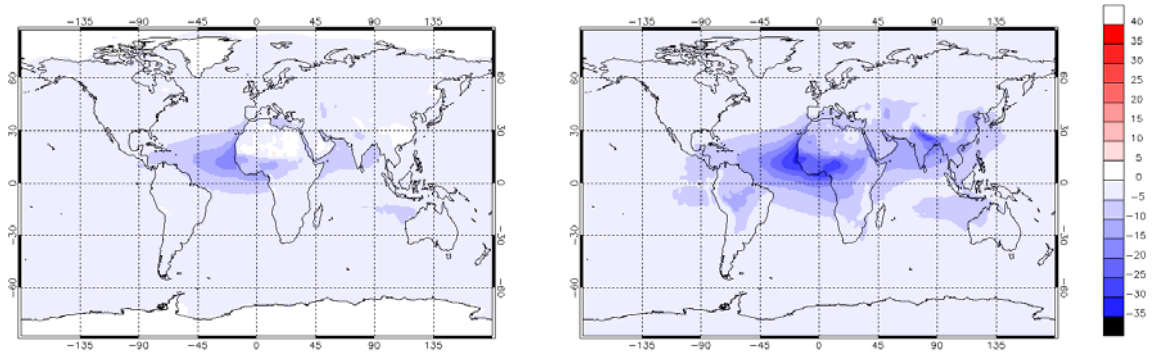

Figure 15 Instantaneous direct radiative forcing due to aerosols at the top of the atmosphere (left) and at the surface (right). Shown here are deacadal annual mean values from the base case simulation. [Units: W m^{-2}]

Figure 16 shows the total radiative forcing difference between the "MC on" and "MC off" simulations and thus gives an indication about the importance of megacity aerosol emissions on the climate system. Net reductions of the surface shortwave irradiance of up to -23 Wm^{-2} are found over the Ganges region and over China. At the top of the atmosphere, megacity emissions exert a much smaller influence which is predominantly positive (up to +3.1 W m^{-2} over China).Of the other world regions with megacity emissions, only Africa yields a noticeable impact on the radiative balance. Here, TOA forcing is enhanced by up to 1 W m^{-2} while surface radiation is reduced by up to -3.1 Wm^{-2}. The radiative forcing changes for Europe are shown in Figure 17. The small signal of megacity emission in Europe leads to a slight cooling effect over western Europe and the North Atlantic while it exacerbates warming in the Mediterranean region. Note that the simulation does include indirect aerosol effects so that this net radiation change includes the changes in cloud properties which are further analyzed below.

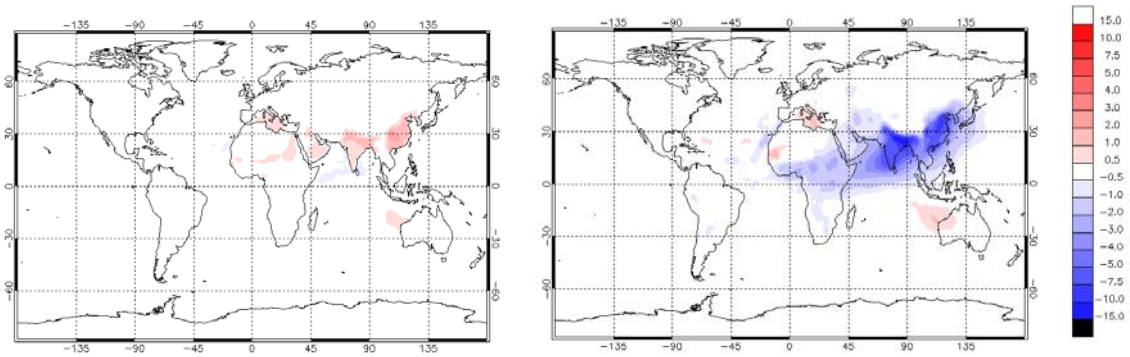

Figure 16 Effect of megacity emissions (see Figure 10) on the instantaneous direct aerosol radiative forcing at the top of the atmosphere (left) and at the surface (right). The figures display the "MC on" minus "MC off" results. [Units: W m^{-2}]

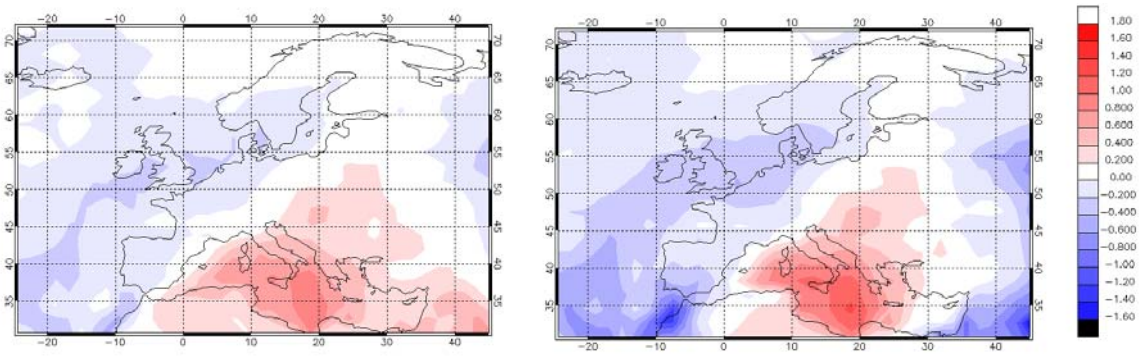

Figure 17 Same as Figure 14, but for Europe only. Note the different color scale. [Units: W m^{-2}]

In the table below we list the global average aerosol radiative forcing terms from the reference and sensitivity simulation, respectively. As discussed above the megacity emissions induce additional cooling at the surface. The signal at the top of the atmosphere is less clear because the clear sky radiative forcing calculation yields a small cooling effect while the all-sky calculation (including clouds) exhibits a small warming effect.

	MC off	MC on
Shortwave clear sky forcing TOA [W m^{-2}]	-4.13	-4.16
Shortwave total forcing TOA [W m^{-2}]	-2.42	-2.38
Shortwave clear sky forcing SUR [W m^{-2}]	-5.81	-6.22
Shortwave total sky forcing SUR [W m^{-2}]	-3.94	-4.25
Longwave clear sky forcing TOA [W m^{-2}]	0.37	0.37
Longwave total forcing TOA [W m^{-2}]	0.22	0.22
Longwave clear sky forcing SUR [W m^{-2}]	1.62	1.62
Longwave total sky forcing SUR [W m^{-2}]	1.03	1.03

Table 3 Global mean and decadal mean aerosol forcing terms of the MC on and MC off simulations, respectively

The aerosol emissions from megacities tend to increase large-scale precipitation in large regions of the tropical and subtropical belt, while they reduce precipitation in some areas of the North Pacific and the Indian Ocean as shown in Figure 18. Due to the short episode of the simulation and the lack of ensemble simulations, these results should be treated with care as they are not statistically robust.

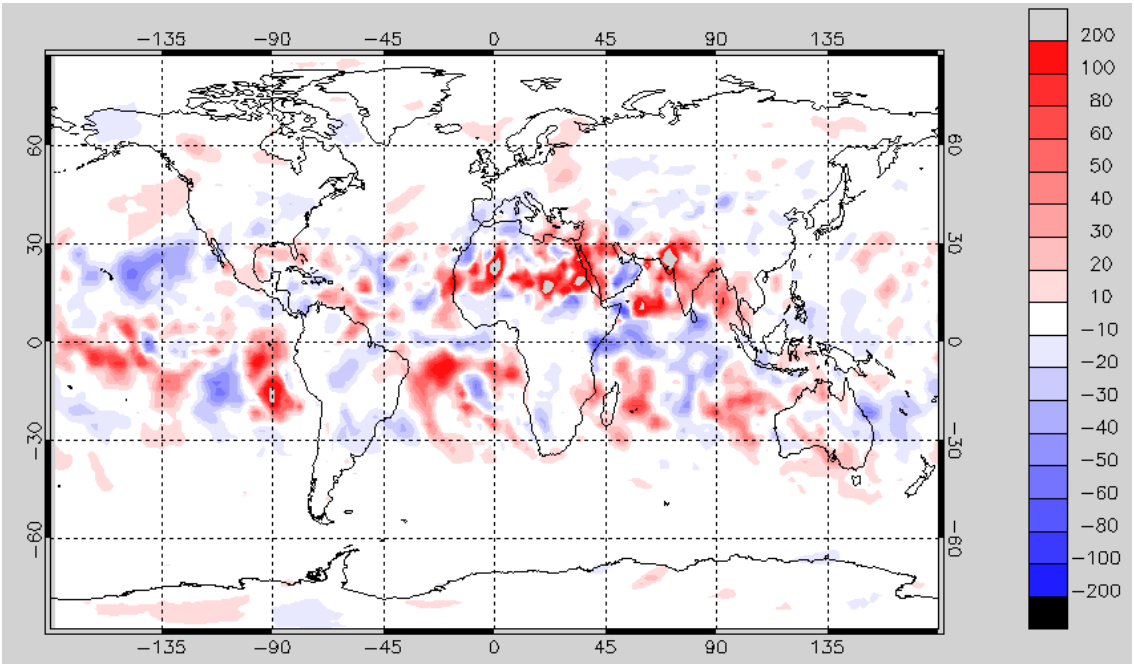

Figure 18 Relative changes (in %) in large-scale precipitation due to megacity aerosol emissions.

Humidity changes due to megacity emissions are shown in Figure 19. While the atmospheric water content near the surface tends to decrease over large parts of the northern mid latitudes with megacity aerosol emissions turned on, India and Australia would experience somewhat more humid air according to these simulations. In the middle troposphere the megacity aerosols generally tend to reduce humidity.

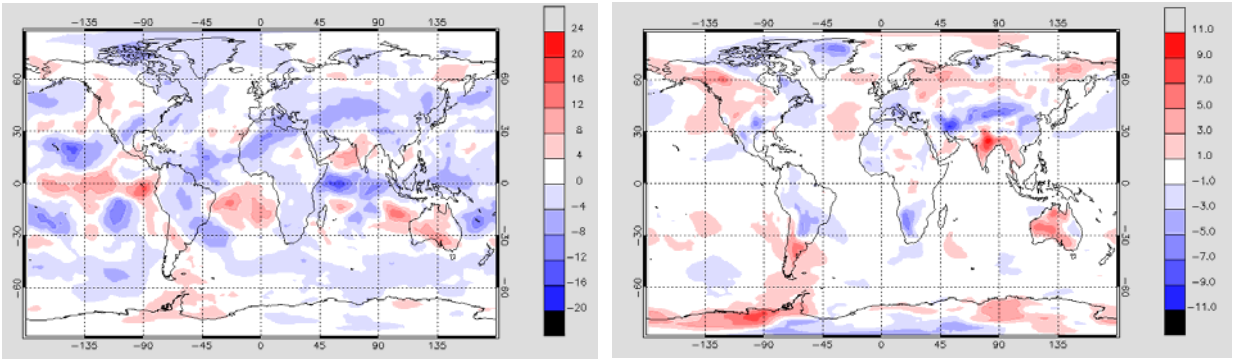

Figure 19 Relative changes (in %) in atmospheric water content at 450 hPa (left) and at the surface (right) due to megacity aerosol emissions.

Figure 20 displays the cloud droplet number concentration of the reference and sensitivity run, respectively. This exhibits an enormous increase in the CDNC concentration over China due to the aerosol emissions in this region. Elsewhere, the signal is much weaker and statistically less reliable. Figure 21 shows the change in the CDNC concentration over Europe. A significant increase of CDNC at the surface can be seen for England and the BENELUX region. This is consistent with the megacity emissions from these regions (see Figure 14). However, large increases are also found elsewhere in regions which are not directly influenced by such emissions.

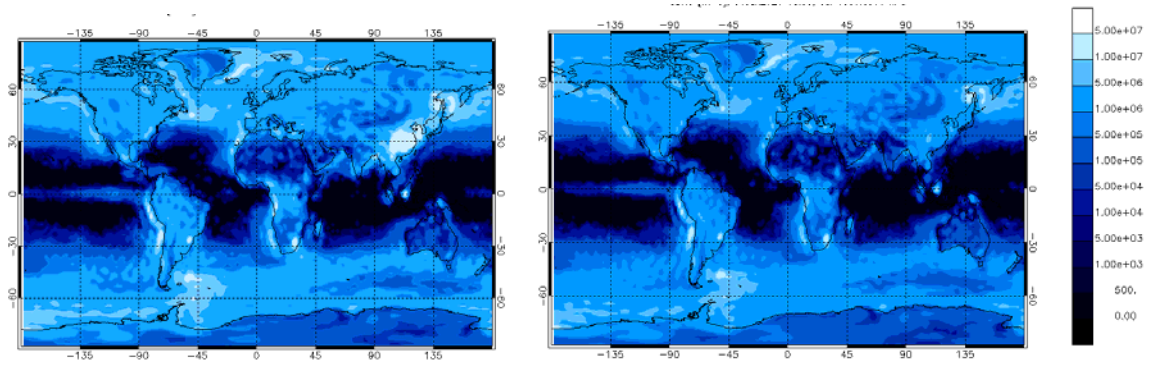

Figure 20 Cloud droplet number concentration at the surface of the reference simulation (left) and the "MC off" run (right). [Units: m^{-3}]

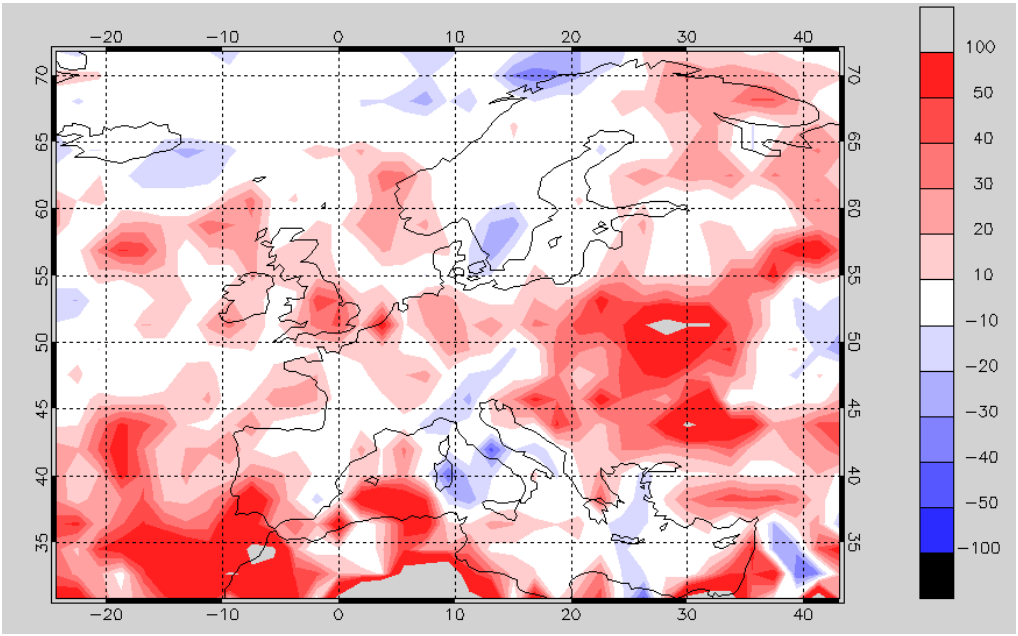

Figure 21 Change in the cloud droplet number concentration at the surface over Europe due to the influence of megacity emissions. [Units: %]

4 Conclusions

Two long-term sensitivity simulations were carried out using a chemistry and an aerosol package for the general circulation model ECHAM5, respectively, in order to assess the impact of meteorological variability on surface ozone concentrations over Europe and the impact of aerosol megacity emissions on the radiative budget of the atmosphere and on cloud properties.

The tropospheric gas-phase chemistry simulations with ECHAM5-MOZ were analyzed with respect to their mean values during the 1990-2008 period and with respect to the variability of surface temperatures and surface ozone concentrations. One simulation with meteorological analyses from the ECMWF ERA-Interim reanalysis was compared to another run which only used prescribed sea surface temperature and sea ice fields. Both runs yielded rather similar mean temperature and ozone distributions, but the variability of summertime ozone concentrations over Eastern Europe was much smaller in the unnudged simulation than in the run with ERA-Interim meteorology. Interest-

ingly, the 5% and 95%-iles of temperature and ozone during the 1990s were rather similar between the two runs. This leads us to conclude that the differences occurred after 2000 (when meteorological fields were taken from operational ECMWF analyses and more extreme summer heat conditions were encountered in Europe). Further analysis is required to confirm this hypothesis. Ozone trend analysis from both simulations shows practically no change over most of Europe while surface ozone increased over the Mediterranean. The unnudged simulation also yields a significant trend over the Iberian Peninsula and in Eastern Europe, which is absent from the nudged run.

For the analysis of climate impacts of megacity emissions we chose to perform two future scenario simulations around the year 2030 based on the ACCMIP RCP8.5 emission scenario. One simulation (reference) used all emissions, while in the other run, all aerosol emissions from "megacity grid boxes" (population density > 150 km^{-2}) were switched off. While this set-up doesn't necessarily provide a realistic description of future megacity emissions, it serves to (i) highlight the major impact regions and (ii) induces signals that are large enough to find statistically robust perturbations. The surface radiative forcing due to megacity aerosol emissions was found to be up to -32 Wm^{-2} while the combination of direct and indirect aerosol effects leads to a slight warming at the top of the atmosphere. Cloud condensation nuclei are generally enhanced due to the megacity contributions and this can be seen even in Europe where the perturbation is relatively small. While this provides a first cursory assessment of the potential impacts of large anthropogenic aerosol sources, more simulations and analyses will be necessary in order to accurately quantify the megacity impacts on climate. Changes in cloud properties in the vicinity of large agglomerations can change weather patterns and therefore influence cloud properties in other regions and it is therefore difficult to disentangle the effect of a specific megacity region in the simulations we have performed for CityZen.

5 Acknowledgements

The authors thank the Jülich Supercomputing Centre for providing the computational resources necessary to carry out the simulations described in this report. C. Richter acknowledges funding from the European Union under the CityZen project (grant 212095). Technical help by S. Schröder and various other colleagues was greatly appreciated.

6 References

A. M. Aghedo, S. Rast and M. G. Schultz (2010). "Sensitivity of tracer transport to model resolution, prescribed meteorology and tracer lifetime in the general circulation model ECHAM5." Atmos. Chem. Phys. **10**(7): 3385-3396.

R. Alley, T. Berntsen, N. L. Bindoff, Z. Chen, A. Chidthaisong, P. Friedlingstein, J. Gregory, G. Hegerl, M. Heimann, B. Hewitson, B. Hoskins, F. Joos, J. Jouzel, V. Kattsov, U. Lohmann, M. Manning, T. Matsuno, M. Molina, N. Nicholls, J. Overpeck, D. Qin, G. Raga, V. Ramaswamy, J. Ren, M. Rusticucci, S. Solomon, R. Somerville, T. F. Stocker, P. Stott, R. J. Stouffer, P. Whetton, R. A. Wood and D. Wratt (2007). Climate Change 2007: The Physical Science Basis, Summary for Policymakers. Geneva, Switzerland, Intergovernmetal Panel on Climate Change (WMO, UNEP)**:** 1-21.

P. Bergamaschi, C. Frankenberg, J. F. Meirink, M. Krol, M. G. Villani, S. Houweling, F. Dentener, E. J. Dlugokencky, J. B. Miller, L. V. Gatti, A. Engel and I. Levin (2009). "Inverse modeling of global and regional CH4 emissions using SCIAMACHY satellite retrievals." J. Geophys. Res. **114**.

G. P. Brasseur, X. Tie, P. J. Rasch and F. Lefèvre (1997). "A three-dimensional simulation of the Antarctic ozone hole: Impact of anthropogenic chlorine on the lower stratosphere and upper troposphere." J. Geophys. Res. **102**(D7): 8909-8930.

S. Deely, D. Dodman, J. Hardoy, C. Johnson, D. Satterthwaite, A. Serafin and R. Waddington (2010). World Disaster Report 2010 - Focus on urban risk. Geneva, Switzerland, International Federation of Red Cross and Red Crescent Societies.

G. Dyner (2008). Climate Wars. Toronto, Canada, Random House of Canada.

A. M. Fiore, F. J. Dentener, O. Wild, C. Cuvelier, M. G. Schultz, P. Hess, C. Textor, M. Schulz, R. M. Doherty, L. W. Horowitz, I. A. MacKenzie, M. G. Sanderson, D. T. Shindell, D. S. Stevenson, S. Szopa, R. Van Dingenen, G. Zeng, C. Atherton, D. Bergmann, I. Bey, G. Carmichael, W. J. Collins, B. N. Duncan, G. Faluvegi, G. Folberth, M. Gauss, S. Gong, D. Hauglustaine, T. Holloway, I. S. A. Isaksen, D. J. Jacob, J. E. Jonson, J. W. Kaminski, T. J. Keating, A. Lupu, E. Marmer, V. Montanaro, R. J. Park, G. Pitari, K. J. Pringle, J. A. Pyle, S. Schroeder, M. G. Vivanco, P. Wind, G. Wojcik, S. Wu, and A. Zuber (2009), Multi-model Estimates of Intercontinental Source-Receptor Relationships for Ozone Pollution, J. Geophys. Res. 114, D04301, doi:10.1029/2008JD010816.

L. Ganzeveld and J. Lelieveld (1995). "Dry deposition parameterization in a chemistry general circulation model and its influence on the distribution of reactive trace gases." Journal of Geophysical Research **100**: 20999-21012.

V. Grewe, D. Brunner, M. Dameris, J. L. Grenfell, R. Hein, D. Shindell and J. Staehelin (2001). "Origin and variability of upper tropospheric nitrogen oxides and ozone at northern mid-latitudes." Atmospheric Environment **35**(20): 3421-3433.

A. Guenther, T. Karl, P. Harley, C. Wiedinmyer, P. I. Palmer and C. Geron (2006). "Estimates of global terrestrial isoprene emissions using MEGAN (Model of Emissions of Gases and Aerosols from Nature)." Atmos. Chem. Phys. J1 - ACP **6**(11): 3181-3210.

Ø. Hodnebrog, F. Stordal and T. K. Berntsen (2011). "Does the resolution of megacity emissions impact large scale ozone?" Atmospheric Environment **available online 14 January 2011**.

L. W. Horowitz, S. Walters, D. L. Mauzerall, L. K. Emmons, P. J. Rasch, C. Granier, X. Tie, J.-F. Lamarque, M. G. Schultz, G. S. Tyndall, J. J. Orlando and G. P. Brasseur (2003). "A global simulation of tropospheric ozone and related tracers: Description and evaluation of {MOZART}, version 2." Journal of Geophysical Research **108**(D24): 4784.

J. W. Hurrell, J. J. Hack, D. Shea, J. M. Caron and J. Rosinski (2008). "A New Sea Surface Temperature and Sea Ice Boundary Dataset for the Community Atmosphere Model." Journal of Climate **21**(19): 5145-5153.

M. Koçak, C. Theodosi, P. Zarmpas, U. Im, A. Bougiatioti, O. Yenigun and N. Mihalopoulos (2010). "Particulate matter (PM10) in Istanbul: Origin, source areas and potential impact on surrounding regions." Atmospheric Environment **available online 15 October 2010**.

J. F. Lamarque, T. C. Bond, V. Eyring, C. Granier, A. Heil, Z. Klimont, D. Lee, C. Liousse, A. Mieville, B. Owen, M. G. Schultz, D. Shindell, S. J. Smith, E. Stehfest, J. Van Aardenne, O. R. Cooper, M. Kainuma, N. Mahowald, J. R. McConnell, V. Naik, K. Riahi and D. P. van Vuuren (2010). "Historical (1850-2000) gridded anthropogenic and biomass burning emissions of reactive gases and aerosols: methodology and application." Atmos. Chem. Phys. **10**(15): 7017-7039.

T. Leisner (2005). Aerosols and their Role in the Atmosphere. WE-Heraeus-Summerschool "Physics of the Environment"

S.-J. Lin and R. B. Rood (1996). "Multidimensional Flux-Form Semi-Lagrangian Transport Schemes." Monthly Weather Review: 2046-2070.

J. A. Logan (1999). "An analysis of ozonesonde data for the troposphere: Recommendations for testing 3-D models and development of a gridded climatology for tropospheric ozone." J. Geophys. Res. **104**(D13): 16115-16149.

S. Madronich and S. Flocke (1999). The role of solar radiation in atmospheric chemistry. Handbook of Environmental Chemistry, Environmental Photochemistry. P. Boule, Springer Verlag.

T. E. Nordeng (1994). "Extended versions of the convective parameterization scheme at {ECMWF} and their impact on the mean transient activity of the model in the tropics." ECMWF Technical Memorandum **206**.

H. Price, L. Jaeglé, A. Rice, P. Quay, P. C. Novelli and R. Gammon (2007). "Global budget of molecular hydrogen and its deuterium content: Constraints from ground station, cruise, and aircraft observations." Journal of geophysical research **112**(D22).

W. J. Randel, F. Wu, J. M. Russell, A. Roche and J. W. Waters (1998). "Seasonal Cycles and QBO Variations in Stratospheric CH4 and H2O Observed in UARS HALOE Data." Journal of the Atmospheric Sciences **55**(2): 163-185.

K. Riahi, A. Grübler and N. Nakicenovic (2007). "Scenarios of long-term socio-economic and environmental development under climate stabilization." Technological Forecasting and Social Change **74**(7): 887-935.

C. Richter (2008). Ozone Production in the Atmosphere Simulation Chamber SAPHIR. Jülich, Forschungszentrum Jülich GmbH, Zentralbibliothek, Verlag.

E. Roeckner, G. Bäuml, L. Bonaventura, R. Brokopf, M. Esch, M. Giorgetta, S. Hagemann, I. Kirchner, L. Kornblueh, E. Manzini, A. Rhodin, U. Schlese, U. Schulzweida and A. Tompkins (2003). the atmospheric general circulation model ECHAM5, part I. Hamburg, Max Planck Institute for Meteorology.

E. Roeckner, R. Brokopf, M. Esch, M. Giorgetta, S. Hagemann, L. Kornblueh, E. Manzini, U. Schlese and U. Schulzweida (2006). "Sensitivity of Simulated Climate to Horizontal and Vertical Resolution in the ECHAM5 Atmosphere Model." Journal of Climate **19**(16): 3771-3791.

J. H. Seinfeld and S. N. Pandis (1998). Atmospheric Chemistry and Physics: From Air pollution to Climate change, John Wiley, United States of America.

P. Stier, J. Feichter, S. Kinne, S. Kloster, E. Vignati, J. Wilson, L. Ganzeveld, I. Tegen, M. Werner, Y. Balkanski, M. Schulz, O. Boucher, A. Minikin and A. Petzold (2005). "The aerosol-climate model ECHAM5-HAM." Atmos. Chem. Phys. **5**(4): 1125-1156.

M. Tiedtke (1989). "A Comprehensive Mass Flux Scheme for Cumulus Parameterization in Large-Scale Models." Monthly Weather Review: 1779-1800.